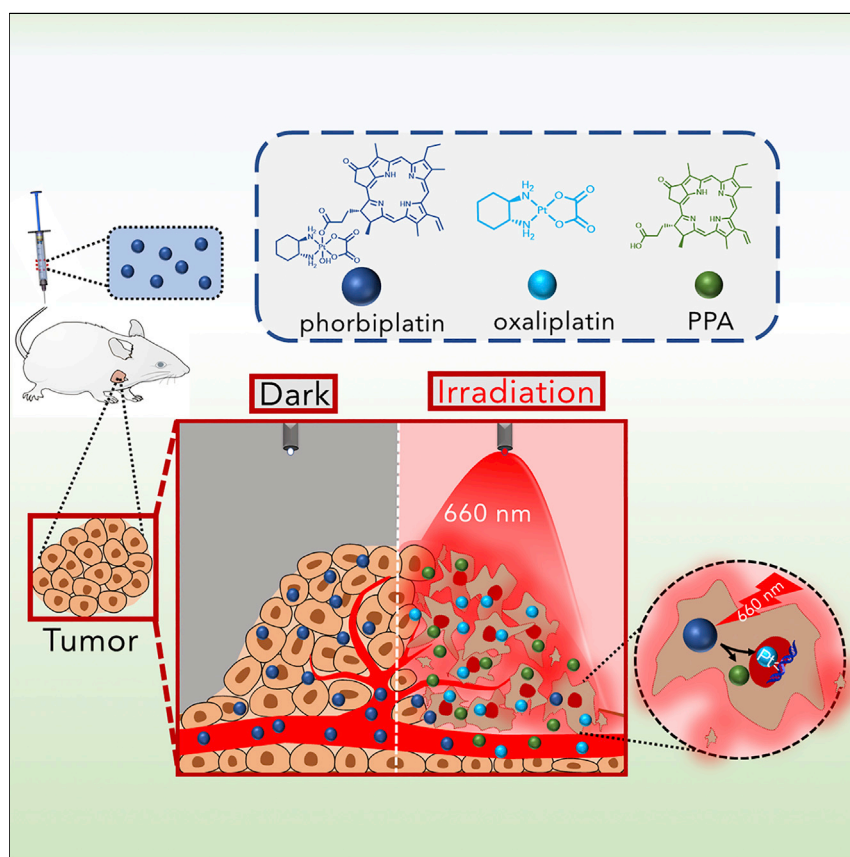


Article

Phorbiplatin, a Highly Potent Pt(IV) Antitumor Prodrug That Can Be Controllably Activated by Red Light



We report the design, evaluation, and photoactivation mechanism of phorbiplatin, a platinum(IV) antitumor prodrug that can be controllably activated by red light. Phorbiplatin maintains its integrity without irradiation, but under irradiation with red light, the prodrug is quickly and efficiently activated, releasing oxaliplatin and PPA. The prodrug shows significant antitumor activity both *in vitro* and *in vivo*.

Zhigang Wang, Na Wang, Shun-Cheung Cheng, ..., Hajime Hirao, Chi-Chiu Ko, Guangyu Zhu

wangzg@szu.edu.cn (Z.W.)
guangzhu@cityu.edu.hk (G.Z.)

HIGHLIGHTS

The first small-molecule Pt(IV) prodrug that can be activated by red light

Study on the unique photoreduction mechanism of the Pt(IV) prodrug

Significantly improved antitumor activity both *in vitro* and *in vivo*

Article

Phorbiplatin, a Highly Potent Pt(IV) Antitumor Prodrug That Can Be Controllably Activated by Red Light

Zhigang Wang,^{1,2,*} Na Wang,^{1,4} Shun-Cheung Cheng,¹ Kai Xu,¹ Zhiqin Deng,^{1,4} Shu Chen,^{1,4} Zoufeng Xu,^{1,4} Kai Xie,³ Man-Kit Tse,¹ Peng Shi,³ Hajime Hirao,¹ Chi-Chiu Ko,¹ and Guangyu Zhu^{1,4,5,*}

SUMMARY

Selective activation of prodrugs within a tumor is particularly attractive because of their low damage to normal tissue. Here, we report the design, photoactivation mechanism, and antitumor activity of a red-light-activatable Pt(IV) prodrug based on oxaliplatin, a first-line clinical antineoplastic. This small-molecule prodrug, designated as phorbiplatin, has controllable activation property: it is shown to be inert in the dark but under short-period irradiation with low intensity of red light (7 mW/cm²), without the need of any external catalyst, phorbiplatin is rapidly reduced to oxaliplatin. The prodrug displays photocytotoxicity that is up to 1,786 times greater than that of oxaliplatin in human carcinoma cells, and it is also significantly active *in vivo*. The controllable activation property and superior antitumor activity of phorbiplatin may suggest a novel strategy for the design of visible light-activatable platinum prodrugs to reduce the adverse effects and conquer drug resistance of traditional platinum chemotherapy.

INTRODUCTION

Controllable activation of prodrugs at the tumor site has been widely explored in cancer chemotherapy, aiming to increase the therapeutic window of conventional chemotherapeutics with limited tumor-targeting property.^{1,2} Both endogenous activators within tumor microenvironments including overexpressed tumor-associated enzymes,³ elevated levels of reactive oxygen species (ROS),⁴ hypoxia⁵ and low pH,⁶ and exogenous activators including catalysts,⁷ light,⁸ and ultrasound⁹ have been utilized to activate prodrugs. Among them, photoactivation is particularly attractive because it can enable the activation of prodrugs in a high spatial and temporal manner.¹⁰ In addition, modern lasers and fiber optics can deliver light to any tissue in the body, making it a solid means for controllable and targeted cancer therapy.¹¹

Despite the great success of platinum chemotherapy including cisplatin, carboplatin, and oxaliplatin in clinics, their toxic side effects, due to non-specific activation of the drugs, as well as drug resistance issues hinder their broader applications.^{12–16} Development of photoactivatable platinum-based anticancer prodrugs is highly appealing. Efforts have been devoted to the design of Pt(IV)-based photoactivatable complexes. Examples include diiodo and diazido Pt(IV) complexes.^{17–20} However, the *in vivo* application of these complexes is limited by slow photoreaction, low stability in physiological conditions, and/or limited activation wavelengths in the region of UVA or blue light to efficiently activate the complexes, which has poor tissue penetration depth. To extend the activation wavelength of the *trans*-diam(m)ine diazido

The Bigger Picture

Currently, most of the small-molecule anticancer drugs used in clinics do not have controllable activation properties, leading to undesired side effects. Anticancer drugs with “on-site” activation properties are highly demanded. Here, we report the development of a small-molecule anticancer prodrug that can be controllably activated by a red light. The prodrug is stable in the dark even in a reducing environment and shows minimum dark toxicity to the cells. Under irradiation with low intensity of red light, the prodrug utilizes a unique photoactivation mechanism to be quickly and efficiently activated, releasing oxaliplatin, a widely used antineoplastic agent. The activated prodrug displays significantly increased cytotoxicity in human cancer cells compared with oxaliplatin, and it is able to kill tumor cells much more efficiently than oxaliplatin in a mouse tumor model. Our work significantly contributes to the development of photoactivatable anticancer prodrugs, especially by red light.

Pt(IV) complexes, upconversion nanoparticles (UCNPs), which are able to convert near-infrared (NIR) light to UV light, have been conjugated with the Pt(IV) complexes to indirectly activate them.^{21–23} However, the photoactivation efficiency via UCNPs is low; the activation needs a high power laser and a long irradiation time. Small-molecule platinum prodrugs that are stable in physiological conditions and can be quickly activated by red or NIR light are highly desired.

Here, we report the design, mechanistic investigation, and antitumor activity of a small-molecule Pt(IV) prodrug that can be activated by red light in a controllable fashion. We have designed a photoactivatable oxaliplatin-based Pt(IV) prodrug, taking advantage of the fact that Pt(IV) complexes have an octahedral geometry in which two axial ligands can tune the properties of the complexes and the saturated coordination sphere gives low reactivity and side effects.^{24–26} This prodrug is kinetically stable in the presence of cellular reducing agents but can be quickly activated under low-power red-light irradiation. This prodrug, proposed to function in a unique photoactivation mechanism, shows significant antitumor activity both *in vitro* and *in vivo*. We believe this strategy will open a window for the development of Pt(IV) prodrugs with controllable activation properties and low side effects.

RESULTS AND DISCUSSION

Rational Design of a Red Light Activatable Pt(IV) Prodrug

To build up a Pt(IV) prodrug that can be efficiently activated by visible light, especially red light, a photo-absorber with strong absorption in the red-light region is needed to collect the energy from light, and the photo-absorber may transfer energy to the Pt center to facilitate the reduction. Indeed, the excited state of photo-absorbers has been shown to regulate redox reactions through energy or electron transfer.^{27,28} Bearing this in mind, we rationally designed a red-light activatable Pt(IV) prodrug, phorbiplatin $\{[Pt(DACH)(PPA)(OH)(ox)]\}$, DACH = (1R,2R)-1,2-diaminocyclohexane, ox = oxalate), in which the pyropheophorbide a (PPA) ligand is located at the axial position of the oxaliplatin-based Pt(IV) prodrug (Figure 1A). PPA has the advantage of high absorbance around 650 nm, with a high quantum yield of singlet oxygen.^{29,30} PPA and its derivatives have been used as photosensitizers in photodynamic therapy and photo-catalysts in several redox reactions through electron transfer under irradiation.^{31–35} In addition, PPA derivatives have been conjugated to platinum(II) drugs to elicit promising anticancer effects.^{36–39} The oxaliplatin scaffold was chosen based on the findings that tetracarboxylato Pt(IV) compounds are generally stable toward reduction.^{40–42} This prodrug supposedly exists in its intact Pt(IV) form in the dark but is activated to release oxaliplatin and PPA under irradiation of red light. Such a stable Pt(IV) prodrug holds promise for minimizing the side effects that originate from non-specific activation of the prodrug by cellular reductants.

Preparation and Characterization of Phorbiplatin

The oxaliplatin-based Pt(IV) scaffold $[Pt(DACH)(OH)_2(ox)]$ was prepared as previously described, and the *N*-hydroxysuccinimide (NHS) ester of PPA was obtained.⁴³ The ester subsequently reacted with $[Pt(DACH)(OH)_2(ox)]$ to yield phorbiplatin (Figure S1). The purity of the prodrug is 96%, as determined by analytical reversed-phase HPLC (RP-HPLC, Figure S2). The prodrug was characterized spectroscopically by ESI-HRMS, ¹H, ¹³C, and ¹⁹⁵Pt NMR, UV-Vis, and fluorescence spectroscopy (Figures S3–S8).

¹Department of Chemistry, City University of Hong Kong, Hong Kong SAR, P. R. China

²School of Pharmaceutical Sciences, Health Science Center, Shenzhen University, Shenzhen 518060, P. R. China

³Department of Biomedical Engineering, City University of Hong Kong, Hong Kong SAR, P. R. China

⁴City University of Hong Kong Shenzhen Research Institute, Shenzhen 518057, P. R. China

⁵Lead Contact

*Correspondence: wangzg@szu.edu.cn (Z.W.), guangzhu@cityu.edu.hk (G.Z.)

<https://doi.org/10.1016/j.chempr.2019.08.021>

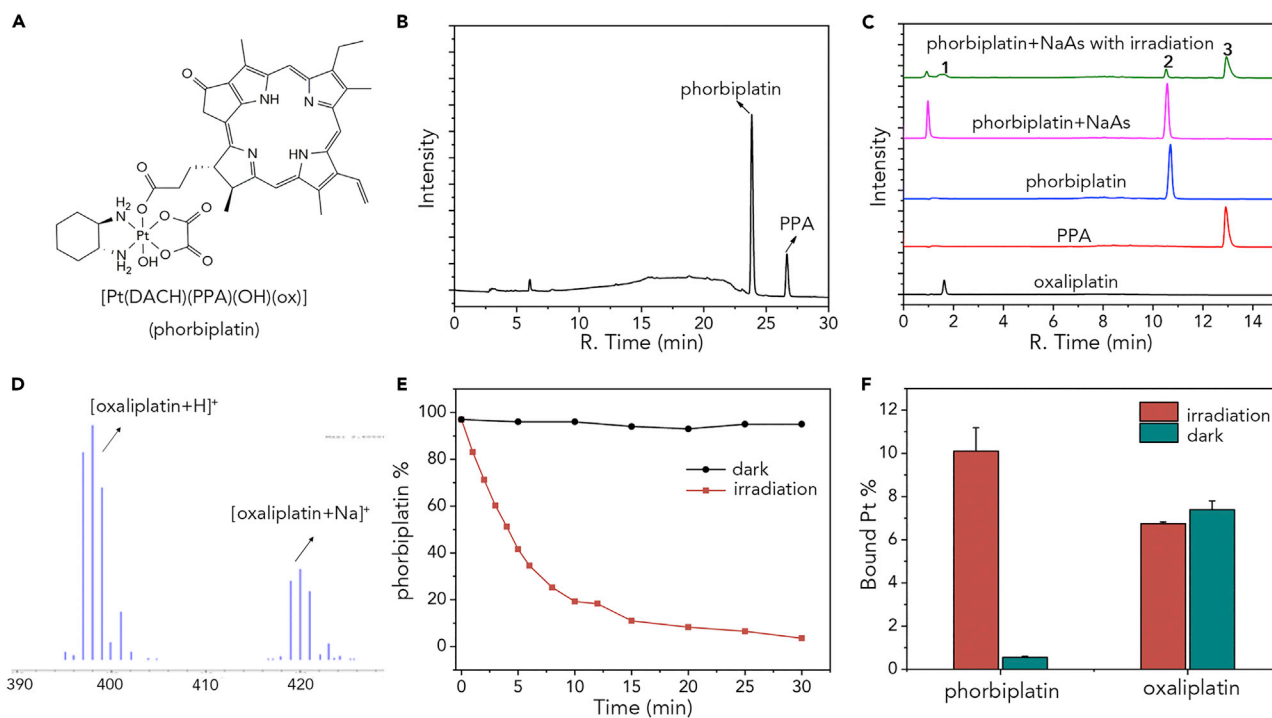


Figure 1. Chemical Structure, Stability, Activation Property, and DNA Binding Ability of Phorbiplatin

(A) Chemical structure of phorbiplatin.

(B) RP-HPLC (254 nm) chromatograms of cell lysate of A2780 cells treated with phorbiplatin (5 μ M) for 8 h.

(C) RP-HPLC (254 nm) chromatograms of oxaliplatin (50 μ M); PPA (50 μ M); phorbiplatin (50 μ M) in the dark; phorbiplatin with 1 equiv. sodium ascorbate (NaAs) (50 μ M) in the dark; and phorbiplatin with 1 equiv NaAs (50 μ M) under irradiation (650 nm, 7 mW/cm²) for 10 min. The compounds were incubated at room temperature in a PBS buffer (pH 7.4) containing 5% acetonitrile and 0.5% DMF. ¹Peak of oxaliplatin; ²peak of phorbiplatin; ³peak of PPA.

(D) ESI-MS (positive mode) results of phorbiplatin in the presence of NaAs under irradiation at the retention time of 1.8 min (indicated as 1 in Figure C) in the m/z range of 390–430, corresponding to [oxaliplatin+H]⁺, calculated at 398.06, found 398 and [oxaliplatin+Na]⁺, calculated at 420.05, found 420.

(E) Time-dependent reduction of phorbiplatin (10 μ M in a PBS buffer containing 1 mM ascorbate) under irradiation (650 nm, 7 mW/cm²) or kept in the dark. Also, see Figure S21.

(F) Percentage of Pt bound to ct-DNA. Phorbiplatin or oxaliplatin (10 μ M) was incubated with ct-DNA (150 μ g), the mixture was kept in the dark or irradiated (650 nm, 7 mW/cm², 30 min), and then the system was further incubated in the dark at 37°C for 24 h (mean \pm SD; n = 2).

Stability of Phorbiplatin

We first examined the stability of phorbiplatin in phosphate buffered saline (PBS, pH = 7.4) in the dark by RP-HPLC. As shown in Figure S9, after incubation for 24 h at 37°C, 96% of phorbiplatin still remained, indicating the high stability of the compound. In the presence of 1 mM ascorbate (100 equiv.), 89% of phorbiplatin remained after 24 h, indicating that the prodrug is quite stable in the dark, even in the presence of the reducing agent (Figure S10). We also prepared the di-carboxylato derivative of phorbiplatin for comparison. The reaction of phorbiplatin with acetic anhydride yields acetylated phorbiplatin (Ac-phorbiplatin) (Figure S11), the target compound, which was characterized by ESI-HRMS, ¹H, ¹³C, and ¹⁹⁵Pt NMR (Figures S12–S16). Ac-phorbiplatin was stable in PBS buffer after incubation for 24 h (Figure S17). In the presence of ascorbate, however, 55% of Ac-phorbiplatin was reduced after incubation for 24 h (Figure S18). Therefore, Ac-phorbiplatin was not considered any further. The stability of phorbiplatin in the presence of another reducing agent, 2-(N-morpholino)ethanesulfonic acid (MES) was tested, and phorbiplatin also remained in its intact form after 24 h at 37 °C (Figure S19). We further tested the stability of phorbiplatin in cells. Cell lysate of A2780 human ovarian carcinoma cells treated with phorbiplatin for 8 h was analyzed by RP-HPLC (Figure 1B). The ratio of the peaks representing phorbiplatin and PPA in the lysate

is 4:1, indicating that 80% of phorbiplatin is kept intact in cells, although there is a possibility that other forms of phorbiplatin metabolite in cells are undetectable from HPLC.

Photoactivation Properties of Phorbiplatin

The photoactivation property of phorbiplatin was subsequently investigated. When a solution of phorbiplatin containing ascorbate was irradiated by red light at 650 nm at a low power density of 7 mW/cm², the height of the peak of phorbiplatin in the HPLC chromatogram quickly decreased, and the peak heights for PPA and oxaliplatin increased simultaneously, indicating the reduction of Pt(IV) to Pt(II) along with the dissociation of the axial PPA ligand (Figure 1C). The formation of oxaliplatin and oxidized ascorbate was further confirmed by ESI-MS (Figures 1D and S20). After irradiation for 10 min, 81% of phorbiplatin was reduced, and most of the complexes were reduced within 30 min (Figures 1E and S21). Irradiation of phorbiplatin in the absence of ascorbate also resulted in the release of PPA and oxaliplatin, although the reaction speed was much slower (Figures S22 and S23). This effect might be because the PPA ligand itself acts as a weak reductant through decomposition under irradiation, as the degradation products were observed in the HPLC chromatogram as small peaks at the retention time of 4 min and 12.5 min (Figure S23).⁴⁴

Photoreduction Mechanism of Phorbiplatin

We further studied the mechanism of the photoreduction. Since no spectral overlap was observed between the emission band of PPA ($\lambda_{em} = 671$ nm) and the absorption of the dihydroxido Pt(IV) compound [Pt(DACH)(OH)₂(ox)] (Figure S24), direct energy transfer is not likely to occur between PPA and the Pt(IV) center. As PPA is able to regulate redox reactions through photo-induced electron transfer (PET), conjugation of PPA at the axial position of Pt(IV) may result in a direct electron transfer from the excited state of PPA to the Pt(IV) center under irradiation. Using PPA in dimethylformamide (DMF; $\Phi_F = 0.31$) as a reference,⁴⁵ the quantum yield of phorbiplatin is determined to be 0.32 in DMF, which is similar to that of PPA. In addition, the fluorescence lifetimes of phorbiplatin and PPA in PBS buffer containing DMF are 7.09 ns and 7.08 ns, respectively (Figure S25). The similar quantum yield and emission lifetime suggest that the singlet excited state of PPA is not directly involved in the reduction process, excluding the possibility of a direct electron transfer from the singlet excited state of PPA to the Pt(IV) center under irradiation.

Given the observations that the photoreduction process of phorbiplatin is much more efficient in the presence of ascorbate (Figures S21 and S22) and that ascorbate is able to reduce PPA analogs to its reduced forms including π radical anion under irradiation through PET,^{46–50} we hypothesized that ascorbate might first reduce the PPA moiety within phorbiplatin, and then the reduced PPA further reduces the Pt(IV) center. To corroborate this hypothesis, we first investigated the photo-induced reduction of PPA in the presence of ascorbic acid. Degassed solutions were used to prevent the auto-oxidation of reduced products by oxygen. Pyridine containing water was chosen as the solvent due to the observation that the reduced form of PPA analogs has a long life in it.^{46,51} As shown in Figure S26A, the spectra of free PPA did not change significantly upon irradiation. Notably, in the presence of ascorbic acid, the spectra of PPA changed rapidly under irradiation, indicating the formation of reduced products. The differential absorbance of irradiated PPA in the presence of ascorbic acid (Figure S26C) is similar to that of mono-reduced PPA π radical anion obtained from electrochemical reduction (Figure S27B), implying that mono-reduced PPA

π radical anion is the main reduced product. Return to darkness led to the recovery of the spectral changes, which is due to the back-reaction of reduced PPA with the oxidized ascorbic acid (Figure S26D). We then studied the cyclic voltammetry of PPA and phorbiplatin in DMF, and the redox potentials are reported versus the $E_{1/2}$ of Fc^+/Fc . As shown in Figure 2A, the reduction potentials ($E_{1/2}$) of free PPA to PPA π radical anion ($PPA^{\bullet-}$) and PPA π radical dianion ($PPA^{\bullet 2-}$) are -1.51 and -1.81 V, respectively. For phorbiplatin, the respective potentials associated with the PPA moiety are slightly higher at $E_{1/2} = -1.47$ and -1.79 V, respectively. A new irreversible reduction peak at $E_p = -1.32$ V represents the reduction of Pt(IV) (Figure 2B), which is comparable to the values reported for other mono-carboxylato oxaliplatin-based Pt(IV) prodrugs.⁴⁰ By employing these data, we estimated the thermodynamic driving force, ΔG_{PET}^0 , for PET between the ascorbate and the excited PPA using the well-known Rehm-Weller equation (see the electrochemistry studies and energetics considerations in the Supplemental Information). The estimated ΔG_{PET}^0 values for the reactions of ascorbate with the singlet excited state and the triplet excited state of PPA to yield $PPA^{\bullet-}$ are -0.64 and -0.16 eV, respectively, indicating the PET reduction of PPA to $PPA^{\bullet-}$ by ascorbate is thermodynamically favorable in both its singlet and triplet excited states. The ΔG_{ET} of electron transfer process from $PPA^{\bullet-}$ to Pt(IV) was estimated to be -0.26 eV, indicating that the process is thermodynamically favorable as well.

We further elucidate the mechanism by using emission quenching study and transient absorption spectroscopy. We measured the emission intensity and decay of both PPA and phorbiplatin in the presence of ascorbate. As shown in Figure S28, upon addition of an increased concentration of ascorbate, the emission intensity of neither PPA nor phorbiplatin changed significantly. The emission lifetimes of PPA and phorbiplatin in the presence of ascorbate are identical to those of free PPA and phorbiplatin (Figure S29), respectively. These results indicate that ascorbate does not react with the singlet excited PPA under irradiation. Thus, ascorbate might reduce the triplet excited state of PPA under irradiation. Indeed, the reduction of porphyrin by ascorbate through its triplet excited state has been reported previously.^{51,52} We further measured the nanosecond transient absorption (ns-TA) spectra of PPA and phorbiplatin in degassed solutions. The ns-TA spectra of PPA show ground-state bleaching at 412 nm and excited-state absorption over the range of 440–550 nm (Figure 2C). The spectral features are consistent with the reported triplet state absorption of PPA derivative.⁵³ The decay time of excited-state absorption at 450 nm of PPA is 6.6 μ s from the single exponential fitting (Figure S30A). The ns-TA spectra and decay time at 450 nm of phorbiplatin are similar to those of PPA (Figures 2D and S30B) and could account for the important role of the PPA moiety within phorbiplatin. The ns-TA spectral features of PPA in the presence of ascorbate are similar to those of free PPA (Figures 2E and S31). In stark contrast, compared with free PPA and phorbiplatin, the decay time of absorption of PPA at 450 nm in the presence of ascorbate increases dramatically to 111 μ s (Figure S30C). This long half-life species is reasonably identified as the reduced form of PPA ($PPA^{\bullet-}$) based on our result mentioned above that $PPA^{\bullet-}$ was formed in the presence of ascorbic acid under irradiation as well as in view of previous reports on the spectral features of reduced porphyrins under irradiation and the porphyrin π radical anion has prolonged decay time.^{50,54,55} The difference between $PPA^{\bullet-}$ (Figure 2E) and the triplet excited PPA (Figure 2C) is difficult to be observed in the ns-TA spectra due to the spectral overlap of $PPA^{\bullet-}$ with the PPA triplet absorption.⁵⁶ The ns-TA spectrum of phorbiplatin in the presence of ascorbate (Figure 2F) is similar to that of PPA with ascorbate (Figure 2E), due to the presence of PPA moiety within phorbiplatin. The decay time of phorbiplatin in the

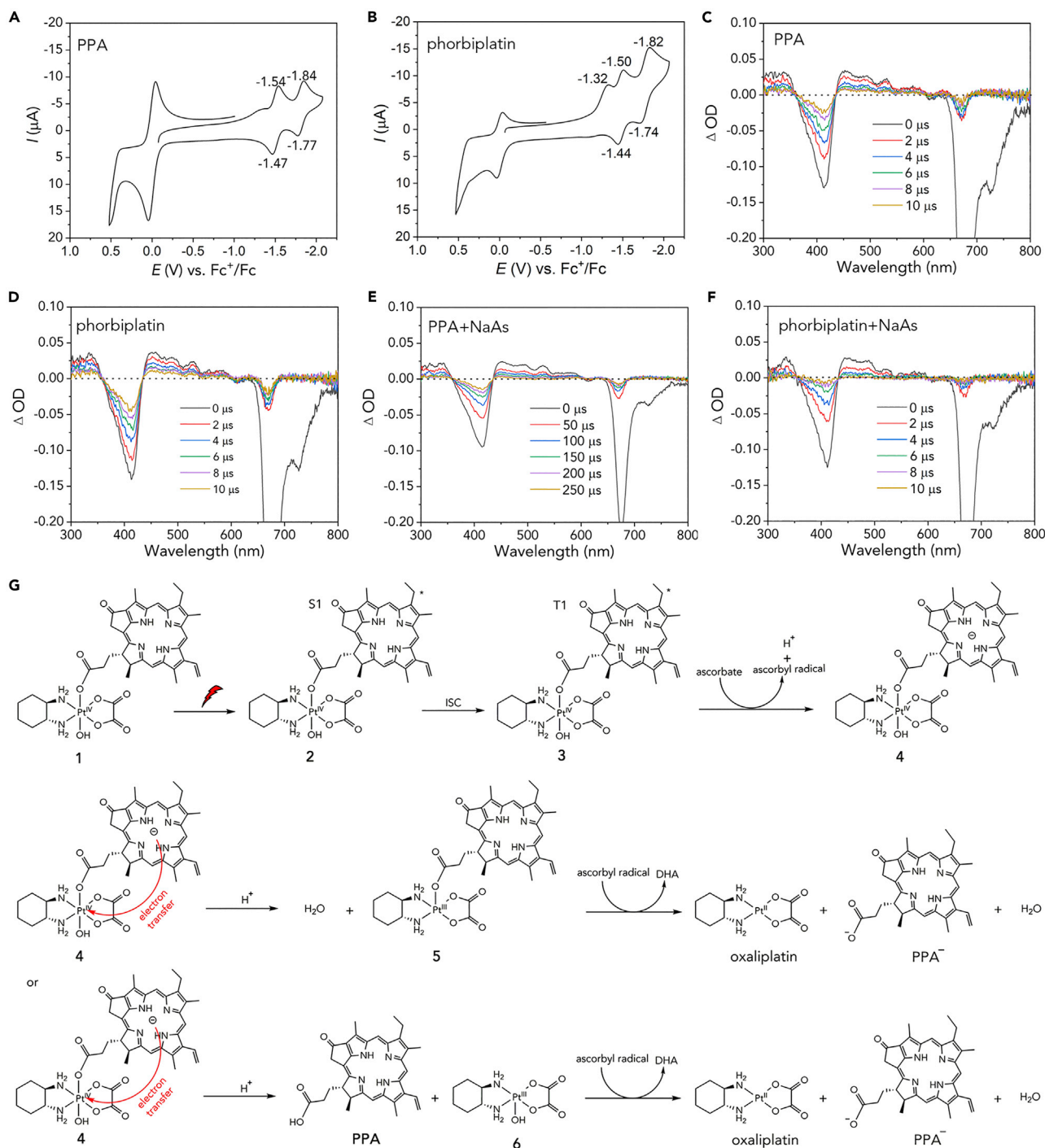


Figure 2. Cyclic Voltammetry, Transient Absorption Spectra, and Proposed Reduction Mechanism of Phorbiplatin

(A) Cyclic voltammogram of PPA in DMF.

(B) Cyclic voltammogram of phorbiplatin in DMF; the data are reported versus the $E_{1/2}$ of Fc^+/Fc .

(C–F) Transient absorption spectra of 10 μM PPA, 10 μM phorbiplatin, 10 μM PPA with 1 mM ascorbate, and 10 μM phorbiplatin with 1 mM ascorbate in PBS buffer containing 50% ACN. Also, see Figure S30. The high decreased absorption around 670 nm at time 0 is due to emission disturbance.

(G) Proposed mechanism of photo-induced reduction of phorbiplatin by ascorbate. Abbreviation is as follows: dehydroascorbic acid, DHA.

presence of ascorbate at 450 nm, however, decreased significantly to 3.0 μs (Figure S30D), indicating a fast reaction of the formed $\text{PPA}^{\bullet-}$ within phorbiplatin. We speculate that this reaction is described as an electron transfer from $\text{PPA}^{\bullet-}$ to the Pt(IV) center, which results in the formation of PPA and Pt(III).

Based on the evidence described above, we propose a photoactivation mechanism of phorbiplatin, which is illustrated in Figure 2G. First, phorbiplatin (1) is excited to its singlet excited state (2) under irradiation, and the singlet excited phorbiplatin (2) goes to its triplet excited state (3) through intersystem crossing (ISC). The energies of 2 and 3 with respect to 1 were estimated by time-dependent density functional theory (TDDFT) calculations as 47.6 and 29.9 kcal/mol, respectively. The triplet excited PPA moiety within phorbiplatin (3) can accept an electron from an electron donor (e.g., ascorbate) to generate a Pt(IV) complex containing ground state PPA π radical anion ($\text{PPA}^{\bullet-}$) (4). Then, $\text{PPA}^{\bullet-}$ transfers one electron to the Pt(IV) center to yield a Pt(III) complex (5) or (6) along with the disassociation of the corresponding axial ligands. The formed Pt(III) complex will then be easily and rapidly reduced to a Pt(II) complex.⁵⁷ The proposed mechanism of action was also probed by density functional theory (DFT) calculations. The relative potential energies of a few species in the reaction processes were calculated. ΔE is -0.8 kcal/mol for the conversion of the Pt(IV) complex 1 to the Pt(III) complex 5, whereas it is -3.4 kcal/mol for the reaction from 5 to the final products. These values suggest that the reactions are thermodynamically favorable. Nevertheless, Pt(III) will not be thermally accessible from Pt(IV), and light is needed here. DFT calculations also suggest that the pathway via 5 is more stable than that via 6. A di-carboxylato Pt(IV) complex is generally thought to have a higher reduction potential (easier to be reduced) than its mono-carboxylato derivative.^{24,58} Therefore, according to our proposed mechanism, Ac-phorbiplatin, a di-carboxylato Pt(IV) complex, might undergo faster photo-induced reduction than phorbiplatin through inner sphere electron transfer. Indeed, the photoreduction rate of Ac-phorbiplatin is significantly faster than that of phorbiplatin. For example, 92% of Ac-phorbiplatin is reduced after irradiation for only 1 min, while the value is as low as 17% for phorbiplatin (Figure S32). This information further supports the validity of our proposed mechanism of the photoreduction process.

Photoreduction of Phorbiplatin by Other Biomolecules

Given the high oxidation ability of excited PPA, many reductants will be able to reduce PPA under irradiation.⁵⁹ Thus, we tested the ability of 2-(*N*-morpholino)ethanesulfonic acid (MES) and glutathione (GSH) as reductants in the photoreduction reaction of phorbiplatin. As shown in Figure S33, MES and GSH promote the reduction of phorbiplatin under irradiation as expected. It has been reported that guanosine 5'-monophosphate (GMP) and adenosine 5'-monophosphate (AMP) in DNA can transfer an electron to PPA under irradiation as well.⁶⁰ We, therefore, co-incubated phorbiplatin with calf thymus (ct)-DNA without other common reductants to investigate the reduction and the subsequent binding to DNA. Theoretically, phorbiplatin is not able to bind covalently to ct-DNA in the dark, and only when it is reduced to oxaliplatin, can the reduced product bind to ct-DNA. As shown in Figure 1F, a trace amount of Pt is detected on DNA in the dark. By contrast, under irradiation, the level of Pt on DNA is similar to that of oxaliplatin, indicating that phorbiplatin is reduced to oxaliplatin. Therefore, DNA serves as a reductant in the system, phorbiplatin is efficiently reduced to oxaliplatin, and the resultant oxaliplatin binds to DNA.

Cellular Accumulation of Phorbiplatin

The biological activity of phorbiplatin was subsequently evaluated. We first tested the cellular accumulation of phorbiplatin by ICP-MS. Platinum accumulation in

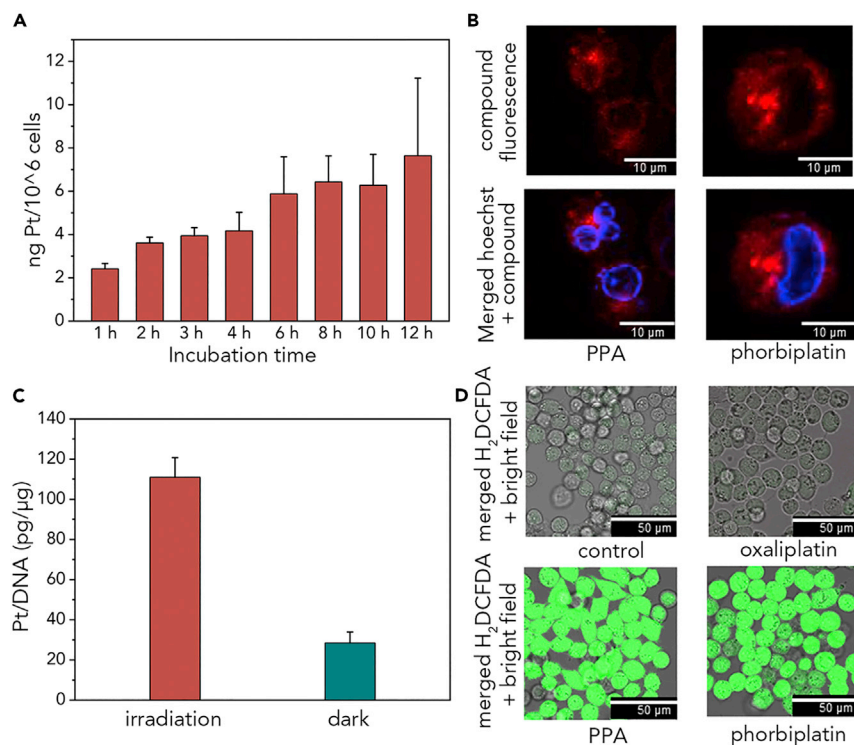


Figure 3. Cellular Accumulation, Genomic DNA Binding Property, and ROS Generation Ability of Phorbiplatin

(A) Time-dependent cellular accumulation of Pt in A2780 cells treated with 0.5 μM phorbiplatin (mean ± SD; n = 3).

(B) Confocal images of A2780 cells treated with 1 μM complexes for 8 h. The blue color corresponds to nuclei stained by 0.2 μM hoechst 33342 (ex = 405 nm, em = 420–480 nm), and the red color is the fluorescence of PPA or phorbiplatin (ex = 405 nm, em = 650–700 nm) (scale bar, 10 μm).

(C) Pt levels in genomic DNA of A2780 cells. The cells were treated with phorbiplatin (0.5 μM) for 8 h, followed by irradiation at 650 nm (7 mW/cm²) for 15 min or in the dark, and further incubated for 8 h before the measurement of Pt in DNA (mean ± SD; n = 3).

(D) Fluorescent images of H₂DCFDA-stained A2780 cells treated with PPA (5 μM) or phorbiplatin (5 μM) for 8 h followed by irradiation at 650 nm (7 mW/cm²) for 5 min (ex = 488 nm, em = 517–527 nm) (scale bar, 50 μm). Also, see Figure S35.

A2780 cells increases dramatically over incubation time before 8 h and remains steady after 8 h (Figure 3A). Thus, an incubation time of 8 h was selected for the following biological assays. The cellular distribution of phorbiplatin was also examined. After treatment of A2780 cells with phorbiplatin at a concentration of 1 μM for 8 h, most of the compound stays in the cytoplasm (Figure 3B).

Cytotoxicity of Phorbiplatin

We subsequently examined the cytotoxicity of phorbiplatin together with oxaliplatin and PPA in platinum-sensitive (A2780) and platinum-resistant (A2780cisR) human ovarian cancer cells. Human breast cancer cells MCF-7 were also used because of their poor response to platinum drugs.⁶¹ These types of cells have been extensively applied in the evaluation of novel metal-based anticancer agents.^{62–64} Cells were treated with the compounds for 8 h, followed by irradiation or incubation in the dark, and the cell viability was measured by MTT assay after 40 h. As shown in Table 1, oxaliplatin shows IC₅₀ values in the typical micromolar range and is not active in A2780cisR cells. Under irradiation, the IC₅₀ values of oxaliplatin do not change significantly from those in the dark, indicating that irradiation has

Table 1. Cytotoxicity of Oxaliplatin, PPA, and Phorbiplatin

| Cell Line | Irradiation | IC ₅₀ (μM) | | | FI ^a |
|-----------|-------------------|-----------------------|-------------|---------------|-----------------|
| | | Oxaliplatin | PPA | Phorbiplatin | |
| A2780 | in the dark | 76 ± 4 | >10 | >10 | |
| | under irradiation | 68 ± 9 | 0.34 ± 0.05 | 0.13 ± 0.01 | 523 |
| A2780cisR | in the dark | 162 ± 9 | >10 | >10 | |
| | under irradiation | 185 ± 8 | 0.23 ± 0.01 | 0.19 ± 0.01 | 974 |
| MCF-7 | in the dark | 110 ± 4.3 | >10 | >10 | |
| | under irradiation | 78.6 ± 8.7 | 0.20 ± 0.02 | 0.044 ± 0.004 | 1786 |
| 4T1 | in the dark | 8.7 ± 0.9 | >10 | >10 | |
| | under irradiation | 7.6 ± 1.3 | 0.16 ± 0.02 | 0.13 ± 0.004 | 58 |
| MRC-5 | in the dark | 122 ± 5.2 | >10 | >10 | |

Cells were treated with complexes for 8 h, followed by irradiation at 650 nm (7 mW/cm²) for 15 min or in the dark. Cell viability was determined by MTT assay at 40 h after irradiation (mean ± SD; n = 3).

^aFI is defined as IC₅₀ of oxaliplatin/IC₅₀ of phorbiplatin.

a negligible effect on the cytotoxicity of oxaliplatin. PPA shows low cytotoxicity to the tested cells in the dark and is active under irradiation, behaving as a typical photosensitizer as previously reported.^{65,66} Phorbiplatin is non-toxic to the tested cells in the dark, and the IC₅₀ value is higher than 10 μM, suggesting the inert properties of this Pt(IV) prodrug before activation. By contrast, under irradiation, phorbiplatin is very active in the tested cells with IC₅₀ values in the nanomolar range. For example, in A2780 cells, the IC₅₀ of phorbiplatin under irradiation is as low as 0.13 μM. Compared with oxaliplatin, the photocytotoxicity of phorbiplatin increases by a factor of 523. Phorbiplatin is also active in platinum-resistant A2780cisR and MCF-7 cells with IC₅₀ values of 0.19 and 0.044 μM, respectively, and the photocytotoxicity of phorbiplatin increases by factors of 974 and 1786 compared with oxaliplatin, respectively. In addition, phorbiplatin is non-toxic to the tested normal human lung fibroblasts MRC-5 in the dark, indicating its low toxicity to normal cells. We also tested the photocytotoxicity of phorbiplatin in 4T1 murine cancer cell line. The tumor growth of 4T1 cells in BALB/c mice closely mimics stage IV human breast cancer, and this cell line has been widely used in antitumor studies.^{67–69} Phorbiplatin shows 58-fold increased photocytotoxicity compared with oxaliplatin in 4T1 cells, indicating its significant activity against late stage breast cancer cells.

Action Mechanism of Phorbiplatin in Cells

More biological assays were carried out to study the fate of phorbiplatin in cells. First, the cellular accumulation levels of Pt in A2780, A2780cisR, and MCF-7 cells treated with phorbiplatin and oxaliplatin for 8 h were measured, and the results are shown in Figure S34. Compared with oxaliplatin, phorbiplatin accumulates more efficiently in the cells. For example, the cellular accumulation levels for phorbiplatin and oxaliplatin in A2780 cells are 6.4 ± 1.2 and 0.9 ± 0.1 ng Pt/10⁶ cells, respectively. This high level of accumulation may be ascribed to the increased lipophilicity of phorbiplatin (LogP = 1.25) compared with that of oxaliplatin (LogP = -1.76).⁷⁰

To confirm whether phorbiplatin can be reduced to oxaliplatin and subsequently bind to genomic DNA in cells, we measured platinum levels in the genomic DNA of A2780 cells treated with phorbiplatin. Under irradiation, the platinum level in DNA is 110 ± 9.7 pg Pt per μg DNA, whereas the value is only 28 ± 5.5 pg Pt per μg DNA in the dark (Figure 3C). This result suggests that a small portion of phorbiplatin may

be reduced in cells in the dark after 16 h, but under irradiation, phorbiplatin is rapidly reduced, resulting in a high level of Pt in genomic DNA.

PPA reportedly acts as a photosensitizer to kill cells by inducing ROS under irradiation.⁷¹ We measured the ROS levels of A2780 cells treated with phorbiplatin to examine its ability to induce ROS using H₂DCFDA as a fluorescent probe. As shown in Figures 3D and S35, compared with untreated cells and cells treated with phorbiplatin or PPA in the dark, cells treated with phorbiplatin or PPA under irradiation show significantly increased fluorescence intensity, suggesting elevated levels of cellular ROS. Therefore, PPA, especially after the dissociation with Pt in cancer cells after irradiation, may also contribute to the cytotoxicity of phorbiplatin. The ability of phorbiplatin to generate ROS was further proved by an *in vitro* cell-free assay based on a chemical probe, 1,3-diphenylisobenzofuran (DPBF) (Figure S36), and the results suggest that phorbiplatin efficiently induces ROS under irradiation.

To further elucidate the contribution of different ROS species in the photocytotoxicity of phorbiplatin, we measured the photocytotoxicity of the compounds in the presence of singlet oxygen inhibitor L-histidine and hydroxyl radical inhibitor D-mannitol. As shown in Table S1, these inhibitors did not change the cytotoxicity of oxaliplatin significantly. In the presence of L-histidine, the photocytotoxicity of PPA decreased, indicating that singlet oxygen plays some roles. In the presence of D-mannitol, however, the photocytotoxicity of PPA decreased more significantly, suggesting that the photocytotoxicity of PPA mainly relies on the generation of hydroxyl radicals. This result is consistent with other reports that a PPA derivative generates more hydroxyl radicals than singlet oxygen.⁵³ For phorbiplatin, in the presence of L-histidine, the photocytotoxicity slightly decreased, and this phenomenon was also observed in the presence of D-mannitol. Therefore, both singlet oxygen and hydroxyl radicals contribute to the photocytotoxicity of phorbiplatin.

We further tested the ability of phorbiplatin to induce apoptosis using an Annexin V/7-aminoactinomycin d (7-AAD) double staining assay, and the result is shown in Figure S37. A2780 cells treated with phorbiplatin under irradiation show high fractions of apoptotic (29.1%) and dead (68.0%) cells compared with all the other groups including untreated cells, cells treated with oxaliplatin, and cells treated with PPA under irradiation. Therefore, phorbiplatin induces cell death through apoptotic pathways.

In vivo Antitumor Activity of Phorbiplatin

Based on the *in vitro* results, we argue that the photocytotoxicity of phorbiplatin is due to its high accumulation in cancer cells followed by the generation of active Pt(II) species together with ROS including singlet oxygen and hydroxyl radicals under irradiation. This multi-action property might result in high antitumor activity *in vivo*. The lack of oxygen in the hypoxic tumor microenvironment will reduce the generation of ROS and the photocytotoxicity of PPA. Our hypothesis is that although the generation of ROS from phorbiplatin may be limited under hypoxia, this prodrug can still generate Pt(II) to exhibit cell-killing effects, which may lead to enhanced antitumor activity compared with oxaliplatin and PPA, or even a mixture.

To corroborate this hypothesis, we further studied the antitumor activity of phorbiplatin *in vivo* using a murine mammary adenocarcinoma 4T1 xenograft model. BALB/c mice bearing the 4T1 tumor model were treated with PPA or phorbiplatin, and the fluorescence of the complex was monitored. As shown in Figure S38, the

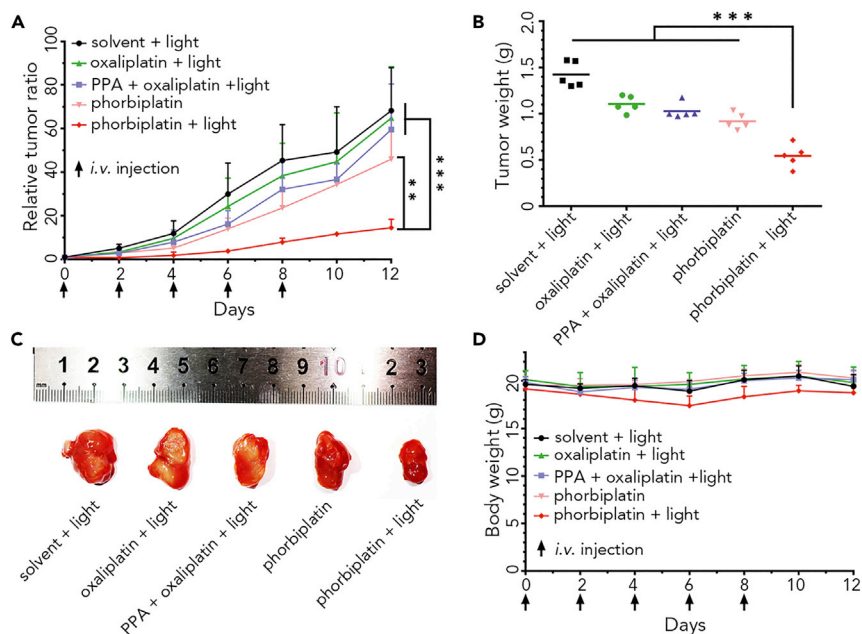


Figure 4. Antitumor Activity of Phorbiplatin In vivo

(A) The growth of 4T1 tumors in a xenograft model treated with various complexes and the relative tumor volumes are presented. Arrows represent the time of complex administration and irradiation. Also, see Figure S39.

(B) Excised tumor weight at the endpoint.

(C) Photographs of excised tumors at the endpoint.

(D) The bodyweight of the mice. The complexes were *i.v.* injected 5 times in total at a dose of 3.5 $\mu\text{mol-Pt/kg}$. 4 h after *i.v.* injection, the tumor sites of irradiation group were irradiated with 660 nm light at a power density of 100 mW/cm^2 for 10 min. The tumor volume of each group was measured every two days for 12 days. (Statistical analysis was carried out using Student's *t* test.

p* < 0.01, *p* < 0.001, mean \pm SD; *n* = 5).

mice showed strong fluorescence near tumors 4 h post-injection of PPA or phorbiplatin. The fluorescence at the tumor site kept decreasing and disappeared after 24 h. Thus, we chose 4 h after injection as the time point for irradiation. BALB/c mice bearing approximately 40 mm^3 4T1 tumors were intravenously injected with different complexes at a dose of 3.5 $\mu\text{mol-Pt/kg}$ every two days for a total of five treatments. After 4 h, tumors were irradiated with red light (660 nm, 100 mW/cm^2) for 10 min. As indicated in Figures 4A and S39, oxaliplatin at this dose exhibited limited effects on the tumor growth, and a mixture of PPA and oxaliplatin with irradiation weakly inhibited the tumor growth. Phorbiplatin in the dark also weakly inhibited the tumor growth, which might be due to the slow reduction of phorbiplatin and the following release of oxaliplatin after a long time *in vivo*. Remarkably, phorbiplatin with irradiation significantly inhibited the tumor growth, with 67% reduction in tumor volume and 62% reduction in tumor weight compared with the control group (Figures S39, 4B, and 4C). These results suggest significantly improved *in vivo* antitumor effects of phorbiplatin compared with oxaliplatin or even a mixture of PPA and oxaliplatin. In addition, the bodyweight of the mice treated with phorbiplatin did not change significantly, highlighting the safety of phorbiplatin (Figure 4D). Moreover, histological analysis (H&E staining) shows that tumor damage occurs more significantly in the phorbiplatin-treated group under irradiation than other groups, suggesting the superior antitumor activity of phorbiplatin (Figure S40). Besides, the results of H&E staining in Figure S40 show that there is liver damage in the mice treated with the mixture of oxaliplatin and PPA under irradiation, raising a

safety concern of the mixture. By contrast, no liver damage was found in the mice treated with phorbiplatin under irradiation, and the other organs are also in good conditions. These results further confirmed the safety of phorbiplatin.

In conclusion, to the best of our knowledge, we developed the first small-molecule Pt(IV) prodrug that can be efficiently and controllably activated by red light in a spatial and temporal fashion. This prodrug is stable in the dark, even in the presence of reductants. Upon red light irradiation, the prodrug is reduced rapidly to oxaliplatin and PPA. Studies on the photoactivation process indicate that the prodrug utilizes a unique mechanism to be photo-reduced: after photoactivation to the triplet excited state, PPA is reduced under irradiation in the presence of ascorbate, and the reduced PPA further reduces the Pt(IV) center to initiate the photoreduction process. The PPA axial ligand acts as a "photo-induced redox relay" to transfer electrons to the Pt(IV) center. To the best of our knowledge, this is also the first example of a small-molecule Pt(IV) prodrug containing a functionalized axial ligand that can facilitate the electron transfer process from a reducing agent to the Pt center under irradiation. The prodrug shows negligible toxicity to cells in the dark, while upon irradiation, it exhibits a remarkable ability to kill cancer cells with up to a 1,786-fold increase in photocytotoxicity compared with oxaliplatin. Mechanistic investigations indicate that oxaliplatin and PPA resulting from the prodrug activation induce DNA damage and ROS species, respectively, to effectively kill cancer cells in a combinatorial mode. The prodrug is also much more photoactive *in vivo* against the growth of breast tumor in BALB/c mice compared with oxaliplatin, PPA, and even a mixture of oxaliplatin and PPA. These results confirm that phorbiplatin is an effective red light-activatable anticancer prodrug, which is able to overcome drug resistance issues of traditional platinum drugs. Compared with the recently reported photoactivation of Pt(IV) prodrugs by adding a photocatalyst externally with the irradiation of blue light, phorbiplatin, as a single agent, does not require the delivery of an external catalyst into the tumor region and is applicable *in vivo* due to the utilization of red light.^{72,73} This novel strategy of building photoactivatable platinum prodrugs opens up a new direction for the design of Pt(IV) prodrugs with controllable activation properties. Our current efforts aim to apply this strategy to other photo-absorbers to obtain more potent Pt(IV) anticancer prodrugs.

EXPERIMENTAL PROCEDURES

The experimental procedures are included in the [Supplemental Information](#).

SUPPLEMENTAL INFORMATION

Supplemental Information can be found online at <https://doi.org/10.1016/j.chempr.2019.08.021>.

ACKNOWLEDGMENTS

We thank the Hong Kong Research Grants Council (CityU 11304318 and 11307419), National Natural Science Foundation of China (21877092), City University of Hong Kong (projects 9610369 to H.H. and 9667148 to G.Z.), the Science Technology and Innovation Committee of Shenzhen Municipality (JCYJ20170307091106444), and Shenzhen University (project 2018022) for funding support.

AUTHOR CONTRIBUTIONS

G.Z. and Z.W. conceived the project. Z.W. and G.Z. designed the experiments and wrote the manuscript. Z.W. designed and conducted the chemical synthesis, characterization, reduction, and *in vitro* biological assays of phorbiplatin. N.W. carried out

the *in vivo* animal assays. Z.W., S.-C.C., and C.-C.K. performed the transient absorption measurement. K.Xu and H.H. carried out the DFT calculations. Z.X. carried out the ¹H NMR experiments. Z.W. and Z.D. carried out the synthesis and characterization of Ac-phorbiplatin. S.C. measured the fluorescence properties of the compounds. Z.W., N.W., K.Xie, and P.S. carried out the animal imaging assays. M.-K.T. conducted the ¹⁹⁵Pt NMR experiments. All authors edited and approved the final manuscript.

DECLARATION OF INTERESTS

G.Z., Z.W., and Z.X. are listed as inventors on a patent application by City University of Hong Kong describing the preparation and therapeutic use of phorbiplatin. The patent is pending in the USA (application number 15/917,966). The other authors declare no competing financial interests.

Received: August 12, 2018

Revised: April 29, 2019

Accepted: August 22, 2019

Published: September 23, 2019

REFERENCES

- Lakshmanan, S., Gupta, G.K., Avci, P., Chandran, R., Sadasivam, M., Jorge, A.E., and Hamblin, M.R. (2014). Physical energy for drug delivery; poration, concentration and activation. *Adv. Drug Deliv. Rev.* **71**, 98–114.
- Du, B.J., Li, D., Wang, J., and Wang, E.K. (2017). Designing metal-contained enzyme mimics for prodrug activation. *Adv. Drug Deliv. Rev.* **118**, 78–93.
- Zhu, L., Wang, T., Perche, F., Taigind, A., and Torchilin, V.P. (2013). Enhanced anticancer activity of nanopreparation containing an MMP2-sensitive PEG-drug conjugate and cell-penetrating moiety. *Proc. Natl. Acad. Sci. USA* **110**, 17047–17052.
- Kim, E.J., Bhuniya, S., Lee, H., Kim, H.M., Cheong, C., Maiti, S., Hong, K.S., and Kim, J.S. (2014). An activatable prodrug for the treatment of metastatic tumors. *J. Am. Chem. Soc.* **136**, 13888–13894.
- Hunter, F.W., Wouters, B.G., and Wilson, W.R. (2016). Hypoxia-activated prodrugs: paths forward in the era of personalised medicine. *Br. J. Cancer* **114**, 1071–1077.
- Noh, J., Kwon, B., Han, E., Park, M., Yang, W., Cho, W., Yoo, W., Khang, G., and Lee, D. (2015). Amplification of oxidative stress by a dual stimuli-responsive hybrid drug enhances cancer cell death. *Nat. Commun.* **6**, 6907.
- Weiss, J.T., Dawson, J.C., Macleod, K.G., Rybski, W., Fraser, C., Torres-Sánchez, C., Patton, E.E., Bradley, M., Carragher, N.O., and Unciti-Broceta, A. (2014). Extracellular palladium-catalysed dealkylation of 5-fluoro-1-propargyl-uracil as a bioorthogonally activated prodrug approach. *Nat. Commun.* **5**, 3277.
- Lameijer, L.N., Ernst, D., Hopkins, S.L., Meijer, M.S., Askes, S.H.C., Le Dévédec, S.E., and Bonnet, S. (2017). A red-light-activated ruthenium-caged NAMPT inhibitor remains phototoxic in hypoxic cancer cells. *Angew. Chem. Int. Ed.* **56**, 11549–11553.
- Tung, C.H., Han, M.S., Kim, Y., Qi, J., and O'Neill, B.E. (2017). Tumor ablation using low-intensity ultrasound and sound excitable drug. *J. Control. Release* **258**, 67–72.
- Yang, Y., Mu, J., and Xing, B. (2017). Photoactivated drug delivery and bioimaging. *Wiley Interdiscip. Rev. Nanomed. Nanobiotechnol.* **9**.
- Yun, S.H., and Kwok, S.J.J. (2017). Light in diagnosis, therapy and surgery. *Nat. Biomed. Eng.* **1**.
- Wang, D., and Lippard, S.J. (2005). Cellular processing of platinum anticancer drugs. *Nat. Rev. Drug Discov.* **4**, 307–320.
- Kelland, L. (2007). The resurgence of platinum-based cancer chemotherapy. *Nat. Rev. Cancer* **7**, 573–584.
- Rabik, C.A., and Dolan, M.E. (2007). Molecular mechanisms of resistance and toxicity associated with platinating agents. *Cancer Treat. Rev.* **33**, 9–23.
- Galluzzi, L., Senovilla, L., Vitale, I., Michels, J., Martins, I., Kepp, O., Castedo, M., and Kroemer, G. (2012). Molecular mechanisms of cisplatin resistance. *Oncogene* **31**, 1869–1883.
- Dasari, S., and Tchounwou, P.B. (2014). Cisplatin in cancer therapy: molecular mechanisms of action. *Eur. J. Pharmacol.* **740**, 364–378.
- Kratochwil, N.A., Zabel, M., Range, K.J., and Bednarski, P.J. (1996). Synthesis and X-ray crystal structure of *trans,cis*-[Pt(OAc)₂(en)]: a novel type of cisplatin analog that can be photolyzed by visible light to DNA-binding and cytotoxic species *in vitro*. *J. Med. Chem.* **39**, 2499–2507.
- Müller, P., Schröder, B., Parkinson, J.A., Kratochwil, N.A., Coxall, R.A., Parkin, A., Parsons, S., and Sadler, P.J. (2003). Nucleotide cross-linking induced by photoreactions of platinum(IV)-azide complexes. *Angew. Chem. Int. Ed.* **42**, 335–339.
- Mackay, F.S., Woods, J.A., Heringová, P., Kaspárková, J., Pizarro, A.M., Moggach, S.A., Parsons, S., Brabec, V., and Sadler, P.J. (2007). A potent cytotoxic photoactivated platinum complex. *Proc. Natl. Acad. Sci. USA* **104**, 20743–20748.
- Farrer, N.J., Woods, J.A., Salassa, L., Zhao, Y., Robinson, K.S., Clarkson, G., Mackay, F.S., and Sadler, P.J. (2010). A potent *trans*-diimine platinum anticancer complex photoactivated by visible light. *Angew. Chem. Int. Ed.* **49**, 8905–8908.
- Min, Y., Li, J., Liu, F., Yeow, E.K., and Xing, B. (2014). Near-infrared light-mediated photoactivation of a platinum antitumor prodrug and simultaneous cellular apoptosis imaging by upconversion-luminescent nanoparticles. *Angew. Chem. Int. Ed.* **53**, 1012–1016.
- Dai, Y., Xiao, H., Liu, J., Yuan, Q., Ma, P., Yang, D., Li, C., Cheng, Z., Hou, Z., Yang, P., et al. (2013). *In vivo* multimodality imaging and cancer therapy by near-infrared light-triggered *trans*-platinum prodrug-conjugated upconversion nanoparticles. *J. Am. Chem. Soc.* **135**, 18920–18929.
- Xu, S., Zhu, X., Zhang, C., Huang, W., Zhou, Y., and Yan, D. (2018). Oxygen and Pt(II) self-generating conjugate for synergistic photochemo therapy of hypoxic tumor. *Nat. Commun.* **9**, 2053.
- Hall, M.D., Mellor, H.R., Callaghan, R., and Hambley, T.W. (2007). Basis for design and development of platinum(IV) anticancer complexes. *J. Med. Chem.* **50**, 3403–3411.
- Johnstone, T.C., Suntharalingam, K., and Lippard, S.J. (2016). The next generation of platinum drugs: targeted Pt(II) agents, nanoparticle delivery, and Pt(IV) prodrugs. *Chem. Rev.* **116**, 3436–3486.

26. Wang, X., and Guo, Z. (2013). Targeting and delivery of platinum-based anticancer drugs. *Chem. Soc. Rev.* *42*, 202–224.
27. Romero, N.A., and Nicewicz, D.A. (2016). Organic photoredox catalysis. *Chem. Rev.* *116*, 10075–10166.
28. Rybicka-Jasińska, K., Shan, W., Zawada, K., Kadish, K.M., and Gryko, D. (2016). Porphyrins as photoredox catalysts: experimental and theoretical studies. *J. Am. Chem. Soc.* *138*, 15451–15458.
29. Feng, X., Jiang, D., Kang, T., Yao, J., Jing, Y., Jiang, T., Feng, J., Zhu, Q., Song, Q., Dong, N., et al. (2016). Tumor-homing and penetrating peptide-functionalized photosensitizer-conjugated PEG-PLA nanoparticles for chemophotodynamic combination therapy of drug-resistant cancer. *ACS Appl. Mater. Interfaces* *8*, 17817–17832.
30. Stamati, I., Kuimova, M.K., Lion, M., Yahioglu, G., Phillips, D., and Deonarain, M.P. (2010). Novel photosensitizers derived from pyropheophorbide-a: uptake by cells and photodynamic efficiency in vitro. *Photochem. Photobiol. Sci.* *9*, 1033–1041.
31. Duan, X., Chan, C., Guo, N., Han, W., Weichselbaum, R.R., and Lin, W. (2016). Photodynamic therapy mediated by nontoxic core-shell nanoparticles synergize with immune checkpoint blockade to elicit antitumor immunity and antimetastatic effect on breast cancer. *J. Am. Chem. Soc.* *138*, 16686–16695.
32. Ethirajan, M., Chen, Y., Joshi, P., and Pandey, R.K. (2011). The role of porphyrin chemistry in tumor imaging and photodynamic therapy. *Chem. Soc. Rev.* *40*, 340–362.
33. He, C., Duan, X., Guo, N., Chan, C., Poon, C., Weichselbaum, R.R., and Lin, W. (2016). Core-shell nanoscale coordination polymers combine chemotherapy and photodynamic therapy to potentiate checkpoint blockade cancer immunotherapy. *Nat. Commun.* *7*, 12499.
34. Shanmugam, S., Xu, J., and Boyer, C. (2015). Utilizing the electron transfer mechanism of chlorophyll a under light for controlled radical polymerization. *Chem. Sci.* *6*, 1341–1349.
35. Xu, J., Shanmugam, S., Fu, C., Aguey-Zinsou, K.F., and Boyer, C. (2016). Selective photoactivation: From a single unit monomer insertion reaction to controlled polymer architectures. *J. Am. Chem. Soc.* *138*, 3094–3106.
36. Brunner, H., and Obermeier, H. (1994). Platinum(II) complexes with porphyrin ligands—additive cytotoxic and photodynamic effect. *Angew. Chem. Int. Ed.* *33*, 2214–2215.
37. Lottner, C., Bart, K.C., Bernhardt, G., and Brunner, H. (2002). Soluble tetraarylporphyrin–platinum conjugates as cytotoxic and phototoxic antitumor agents. *J. Med. Chem.* *45*, 2079–2089.
38. Lottner, C., Bart, K.C., Bernhardt, G., and Brunner, H. (2002). Hematoporphyrin-derived soluble porphyrin–platinum conjugates with combined cytotoxic and phototoxic antitumor activity. *J. Med. Chem.* *45*, 2064–2078.
39. Brunner, H., and Gruber, N. (2004). Carboplatin-containing porphyrin–platinum complexes as cytotoxic and phototoxic antitumor agents. *Inorg. Chim. Acta* *357*, 4423–4451.
40. Zhang, J.Z., Wexselblatt, E., Hambley, T.W., and Gibson, D. (2012). Pt(IV) Analogs of oxaliplatin that do not follow the expected correlation between electrochemical reduction potential and rate of reduction by ascorbate. *Chem. Commun.* *48*, 847–849.
41. Thiabaud, G., McCall, R., He, G., Arambula, J.F., Siddik, Z.H., and Sessler, J.L. (2016). Activation of platinum(IV) prodrugs by motexafin gadolinium as a redox mediator. *Angew. Chem. Int. Ed.* *55*, 12626–12631.
42. Varbanov, H.P., Valiahd, S.M., Kowol, C.R., Jakupec, M.A., Galanski, M., and Keppler, B.K. (2012). Novel tetracarboxylatoplatinum(IV) complexes as carboplatin prodrugs. *Dalton Trans.* *41*, 14404–14415.
43. Zhang, J.Z., Bonnitcha, P., Wexselblatt, E., Klein, A.V., Najajreh, Y., Gibson, D., and Hambley, T.W. (2013). Facile preparation of mono-, di- and mixed-carboxylato platinum(IV) complexes for versatile anticancer prodrug design. *Chem. Eur. J.* *19*, 1672–1676.
44. Bonnett, R., and Martínez-Botella, G. (2001). Photobleaching of sensitizers used in photodynamic therapy. *Tetrahedron* *40*, 9513–9547.
45. Al-Omari, S., and Ali, A. (2009). Photodynamic activity of pyropheophorbide methyl ester and pyropheophorbide a in dimethylformamide solution. *Gen. Physiol. Biophys.* *28*, 70–77.
46. Bannister, T.T. (1959). Photoreduction of chlorophyll a in the presence of ascorbic acid in pyridine solutions. *Plant Physiol.* *34*, 246–254.
47. Chibisov, A.K. (1969). A flash photolysis study of intermediates in photochemical reactions of chlorophyll. *Photochem. Photobiol.* *10*, 331–347.
48. Suboch, V.P., Losev, A.P., and Gurinovitch, G.P. (1974). Photoreduction of protochlorophyll and its derivatives. *Photochem. Photobiol.* *20*, 183–190.
49. Felix, C.C., Reszka, K., and Sealy, R.C. (1983). Free radicals from photoreduction of hematoporphyrin in aqueous solution. *Photochem. Photobiol.* *37*, 141–147.
50. Richoux, M.C., Neta, P., Harriman, A., Baral, S., and Habright, P. (1986). One- and two-electron reduction of metalloporphyrins. Radiation chemical, photochemical, and electrochemical studies. Kinetics of the decay of π -radical anions. *J. Phys. Chem.* *90*, 2462–2468.
51. Livingston, R., and McCartin, P.J. (1963). Some observations related to the photoreduction of chlorophyll. *J. Am. Chem. Soc.* *85*, 1571–1573.
52. Livingston, R., and Pugh, A.C.P. (1960). Role of the triplet state in the photoreduction of chlorophyll. *Nature* *186*, 969–970.
53. Delanaye, L., Bahri, M.A., Tfibel, F., Fontaine-Aupart, M.P., Mouithys-Mickalad, A., Heine, B., Piette, J., and Hoebeke, M. (2006). Physical and chemical properties of pyropheophorbide-a methyl ester in ethanol, phosphate buffer and aqueous dispersion of small unilamellar dimyristoyl- α -phosphatidylcholine vesicles. *Photochem. Photobiol. Sci.* *5*, 317–325.
54. Neta, P., Scherz, A., and Levanon, H. (1979). Electron transfer reactions involving porphyrins and chlorophyll a. *J. Am. Chem. Soc.* *101*, 3624–3629.
55. Neta, P. (1981). One-electron transfer reactions involving zinc and cobalt porphyrins in aqueous solutions. *J. Phys. Chem.* *85*, 3678–3684.
56. Whitten, D.G., Yau, J.C.N., and Carroll, F.A. (1971). Photochemistry and oxidation-reduction reactions of tin porphyrins. *J. Am. Chem. Soc.* *93*, 2291–2296.
57. McCormick, M.C., Keijzer, K., Polavarapu, A., Schultz, F.A., and Baik, M.H. (2014). Understanding intrinsically irreversible, non-Nernstian, two-electron redox processes: a combined experimental and computational study of the electrochemical activation of platinum(IV) antitumor prodrugs. *J. Am. Chem. Soc.* *136*, 8992–9000.
58. Wilson, J.J., and Lippard, S.J. (2011). Synthesis, characterization, and cytotoxicity of platinum(IV) carbamate complexes. *Inorg. Chem.* *50*, 3103–3115.
59. Mauzerall, D. (1960). The photoreduction of porphyrins and the oxidation of amines by photo-excited dyes. *J. Am. Chem. Soc.* *82*, 1832–1833.
60. Díaz-Espinosa, Y., Crespo-Hernández, C.E., Alegría, A.E., García, C., and Arce, R. (2011). Quenching enhancement of the singlet excited state of pheophorbide-a by DNA in the presence of the quinone carboquinone. *Photochem. Photobiol.* *87*, 275–283.
61. Eckstein, N. (2011). Platinum resistance in breast and ovarian cancer cell lines. *J. Exp. Clin. Cancer Res.* *30*, 91.
62. Knopf, K.M., Murphy, B.L., MacMillan, S.N., Baskin, J.M., Barr, M.P., Boros, E., and Wilson, J.J. (2017). In vitro anticancer activity and in vivo biodistribution of rhenium(I) tricarbonyl aqua complexes. *J. Am. Chem. Soc.* *139*, 14302–14314.
63. Qin, H., Zhao, C., Sun, Y., Ren, J., and Qu, X. (2017). Metallo-supramolecular complexes enantioselectively eradicate cancer stem cells in vivo. *J. Am. Chem. Soc.* *139*, 16201–16209.
64. Venkatesh, V., Mishra, N.K., Romero-Canelón, I., Vernooij, R.R., Shi, H., Coverdale, J.P.C., Habtemariam, A., Verma, S., and Sadler, P.J. (2017). Supramolecular photoactivatable anticancer hydrogels. *J. Am. Chem. Soc.* *139*, 5656–5659.
65. Savellano, M.D., Pogue, B.W., Hoopes, P.J., Vitetta, E.S., and Paulsen, K.D. (2005). Multiepitope HER2 targeting enhances photoimmunotherapy of HER2-overexpressing cancer cells with pyropheophorbide-a immunoconjugates. *Cancer Res.* *65*, 6371–6379.
66. Wang, J., Liu, Q., Zhang, Y., Shi, H., Liu, H., Guo, W., Ma, Y., Huang, W., and Hong, Z. (2017). Folic acid-conjugated pyropheophorbide a as the photosensitizer tested for in vivo targeted photodynamic therapy. *J. Pharm. Sci.* *106*, 1482–1489.

67. Pulaski, B.A., and Ostrand-Rosenberg, S. (2001). Mouse 4T1 breast tumor model. *Curr. Protoc. Immunol.* 2.
68. Qi, J., Chen, C., Zhang, X., Hu, X., Ji, S., Kwok, R.T.K., Lam, J.W.Y., Ding, D., and Tang, B.Z. (2018). Light-driven transformable optical agent with adaptive functions for boosting cancer surgery outcomes. *Nat. Commun.* 9, 1848.
69. Wang, T., Wang, D., Yu, H., Feng, B., Zhou, F., Zhang, H., Zhou, L., Jiao, S., and Li, Y. (2018). A cancer vaccine-mediated postoperative immunotherapy for recurrent and metastatic tumors. *Nat. Commun.* 9, 1532.
70. Rappel, C., Galanski, M., Yasemi, A., Habala, L., and Keppler, B.K. (2005). Analysis of anticancer platinum(II)-complexes by microemulsion electrokinetic chromatography: separation of diastereomers and estimation of octanol-water partition coefficients. *Electrophoresis* 26, 878–884.
71. Zhou, A., Wei, Y., Wu, B., Chen, Q., and Xing, D. (2012). Pyropheophorbide a and c(RGDyK) comodified chitosan-wrapped upconversion nanoparticle for targeted near-infrared photodynamic therapy. *Mol. Pharmaceutics* 9, 1580–1589.
72. Alonso-de Castro, S., Cortajarena, A.L., López-Gallego, F., and Salassa, L. (2018). Bioorthogonal catalytic activation of platinum and ruthenium anticancer complexes by FAD and flavoproteins. *Angew. Chem. Int. Ed.* 57, 3143–3147.
73. Alonso-de Castro, S., Ruggiero, E., Ruiz-de-Angulo, A., Rezabal, E., Mareque-Rivas, J.C., Lopez, X., López-Gallego, F., and Salassa, L. (2017). Riboflavin as a bioorthogonal photocatalyst for the activation of a Pt^{IV} prodrug. *Chem. Sci.* 8, 4619–4625.